# Polarized infrared reflectivity of 2D sea surfaces with two surface reflections

Hongkun Li [a],[*], Nicolas Pinel [b], Christophe Bourlier [a]

[a] *Lunam Université - Université de Nantes - IETR Laboratory, Polytech Nantes, Rue C. Pauc, La Chantrerie, BP 50609, 44306 Nantes Cedex 3, France*
[b] *Alyotech Technologies - Technoparc de l'Aubinière, 2 impasse des Jades, BP 93884, 44388 Nantes Cedex 3, France*

## ARTICLE INFO

## ABSTRACT

Sea surface infrared reflectivity is an important parameter in oceanic remote sensing. Most analytical models consider single surface reflections, and the polarization is usually ignored. However, a loss of energy is reported for large observation angles ($\theta > 50°$) because multiple surface reflections are ignored. This article generalizes the infrared reflectivity derivation of Li et al. (Appl. Opt., Vol. 52, 6100–6111, 2013) for 1D surfaces (2D problems) to 2D surfaces (3D problems), so that the cross-polarization effect can be taken into account. The contributions of one and two successive surface reflections are analyzed separately. The bidirectional reflectivity and the hemispherical reflectivity are studied. It is shown that the sea surface infrared reflectivity is significant for large incidence and observation angles. The energy conservation criterion is then checked. The loss of energy is largely reduced after taking into account two surface reflections.

## 1. Introduction

Sea surface infrared reflectivity $\rho$ receives wide attention in many fields of oceanic remote sensing, e.g. in the estimation of sea surface temperature (Smith et al., 1996), the determination of the sea surface bidirectional reflectance distribution function (BRDF) (Caillault, Fauqueux, Bourlier, Simoneau, & Labarre, 2007; Fauqueux, Caillault, Simoneau, & Labarre, 2009; Ross, Dion, & Potvin, 2005), and the vessel detection (Vaitekunas, Alexan, Lawrence, & Reid, 1996). It corresponds to the ability of the sea surface to reflect the incident energy, thus it depends on the wavelength of the incident (ray) wave, the incidence and the observation directions, and the surface roughness.

While reflectivity is closely related to emissivity $\varepsilon$, their derivations for sea surfaces differ. Specifically, emissivity is derived under a monostatic configuration (one receiver and no emitter) but the derivation of the reflectivity employs a bistatic configuration (one receiver and one emitter).

According to the law of energy conservation, the sum of the reflected and absorbed energies equals the incident energy (for an opaque body), meaning that the sum of the emissivity $\varepsilon$ and hemispherical reflectivity $\rho^{\text{hemi}}$ equals 1. Nalli, Smith, and Huang (2001) and Watts, Allen, and Nightingale (1996) derived the sea surface infrared reflectivity from $\rho^{\text{hemi}} = 1 - \varepsilon$. This method avoids the calculation of the probability of having single or multiple reflections, and it is then simpler. However,

the bidirectional characteristics of the reflectivity cannot be studied with this method. As a result, the surface reflectivity is usually calculated from facet models under a bistatic configuration without deriving the emissivity.

Published analytical facet models of sea surface infrared reflectivity, e.g. Bourlier, Saillard, and Berginc (2001), Caillault et al. (2007), Fauqueux et al. (2009), Ross et al. (2005) and Yoshimori, Itoh, and Ichioka (1994), considered single surface reflection. The shadowing effect due to the surface roughness was evaluated by using a bistatic illumination function. However, when examining the energy conservation criterion with analytical facet models of the sea surface infrared emissivity and reflectivity, a loss of energy was reported for large zenith angles by Yoshimori et al. (1994). A maximum of the loss of energy of the order of 0.04 was found around $\theta \approx 80°$, meaning that about 4% of the incident energy is "lost". The reason is that the energy undergoing multiple surface reflections is not taken into account.

Multiple surface reflections are seldom studied because the probability of their occurrence, which is determined by a bistatic illumination function $S_B^n$ with $n > 1$ reflections, is hard to evaluate. The Monte Carlo ray-tracing method, such as the model of Henderson, Theiler, and Villeneuve (2003) for the emissivity and that of Schott, de Beaucoudrey, and Bourlier (2003) for the reflectivity, is a direct way to study multiple surface reflections and is a good reference for analytical models. The analytical models of Watts et al. (1996), Nalli, Minnett, and Delst (2008) and Nalli et al. (2001) consider double surface reflections. The surface total reflectivity is calculated by $1 - \varepsilon$, where $\varepsilon$ is the surface emissivity including one surface reflection. These models avoid the calculation of a bistatic illumination function

and thus are more simple, but the bidirectional characteristics of the reflectivity cannot be studied. Bourlier, Berginc, and Saillard (2002) developed an analytical bistatic illumination function $S_B^n$ which was still not validated by numerical results. Lynch and Wagner (1970) built an analytical bistatic illumination function with 2 reflections $S_B^2$, with which they calculated the reflected field of an incident wave on a perfectly-conducting rough surface. They proved that the law of energy conservation was better satisfied by considering the second reflection. Li, Pinel, & Bourlier (2013) analytically calculated the sea surface infrared reflectivity with 2 reflections by introducing a new bistatic illumination function $S_B^2$. They proved also that the energy conservation is better satisfied after taking into account multiple surface reflections. Their model considered one-dimensional surfaces (1D surfaces — surfaces vary along 1 direction, 2D problems), thus it is not able to study the cross-polarization effect.

This study extends the model of Li et al. (2013) to two-dimensional surfaces so as to take into account the cross-polarization effect. The sea surface polarized infrared reflectivity is calculated analytically by taking into account the contribution of the first and second surface reflections. The reflectivity with one reflection is calculated following the model of Bourlier et al. (2001). The one with two reflections is calculated by extending the model of Li et al. (2013) to 2D surfaces. The geometric optics (GO) approximation is assumed to be valid in the infrared domain (Li, Pinel, & Bourlier, 2011), under which only specular reflections are considered. The sea surface is modeled as single-valued with a Gaussian slope probability density function (PDF) and a Gaussian height autocorrelation function. Whitecaps and breaking waves are not considered in this model, reducing the applicability of the model to moderate winds.

This article is organized as follows: the reflectivity with one surface reflection is calculated in Section 2, and the one with two reflections is calculated in Section 3. The results of the model are shown in Section 4, in which the law of energy conservation is examined.

## 2. Reflectivity with one reflection

The sea surface reflectivity with one reflection corresponds to the radiance from the sky reflected once by the sea surface. Fig. 1 shows an example of single surface reflection.

A system of coordinates $(x, y, z)$ is defined, with $x$, $y$, $z$ being the up-wind, cross-wind and zenith directions, respectively. The sensor and the emitter are located in the $\hat{s}(\theta, \phi)$ and the $\hat{s}_i^-(\theta_i, \phi_i)$ directions, respectively, where the superscript "$-$" stands for the inverse of
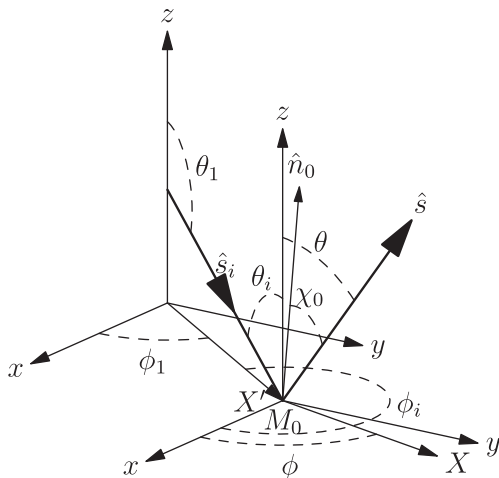
direction. The angles $\theta$ and $\theta_i$ are the zenith angles (within $[0°;$ $90°]$) measured from the zenith, and $\phi$ and $\phi_i$ are the azimuth angles (within $[0°; 360°]$) measured from the up-wind direction (see Fig. 1). For better convenience in the calculations, two new systems of coordinates are defined. The first one $(X, Y, z)$ is defined so that the observation direction $\hat{s}$ belongs to the $Xz$ plane, and the second one $(X', Y', z)$ is defined so that the incidence direction $\hat{s}_i^-$ belongs to the $X'z$ plane. See Fig. 1 for details of the definitions.

### 2.1. $S_B$ with one reflection

Because of the sea surface roughness, shadowing along the incidence and observation directions cannot be ignored when the emitter and/or the sensor are/is close to the horizon. To evaluate the shadowing effect, a bistatic illumination function with one surface reflection $S_B^1$ is employed, which gives the probability that the incident ray is reflected once by one surface point $M_0$. In this article, the inverse path is used, which means that a ray is transmitted by the sensor along $\hat{s}^-$ and is reflected by $M_0$ into the $\hat{s}_i^-$ direction. The extended model of Smith (1967) is used here, given by (Sancer, 1969; Bourlier, Saillard, and Berginc, 2000b):

$$S_B^1\left(\theta, \theta_i, \gamma_{x_0}, \gamma_{y_0}\right) = \frac{\delta(\theta_i^{\mathrm{spe}} - \theta_i)\delta(\phi_i^{\mathrm{spe}} - \phi_i)}{\Lambda(\theta) + \Lambda^-(\theta_i) + 1}, \tag{1}$$

where $\Lambda$ and $\Lambda^-$ correspond to rays propagating toward and away from the positive direction of the horizontal axis (here $X$ and $X'$), respectively, given by (Bourlier et al., 2000b; Li et al., 2011):

$$\Lambda(\theta) = \frac{1}{\mu} \int_\mu^{+\infty} (\gamma - \mu)p_{\gamma_X}(\gamma)d\gamma, \quad \Lambda^-(\theta_i) = \frac{1}{\mu_i} \int_{-\infty}^{\mu_i} (\gamma - \mu_i)p_{\gamma_{X'}}(\gamma)d\gamma, \tag{2}$$

where $\mu = \cot\theta$ and $\mu_i = -\cot\theta_i = \cot\theta_1$ are the slopes of the rays, and $p_{\gamma_X}$ and $p_{\gamma_{X'}}$ are the marginal slope probability density functions (PDF) of the surface along the $X$ and $X'$ directions.

The Dirac delta functions $\delta(\theta_i^{\mathrm{spe}} - \theta_i)$ and $\delta(\phi_i^{\mathrm{spe}} - \phi_i)$ ensure that the ray $\hat{s}^-$ is reflected specularly into the $\hat{s}_i^-$ direction (inverse path). The angles $\theta_i^{\mathrm{spe}}$ and $\phi_i^{\mathrm{spe}}$ are the zenith and azimuth angles of the specular reflection direction $\hat{s}_i^{-,\mathrm{spe}}$ of the ray $\hat{s}^-$.
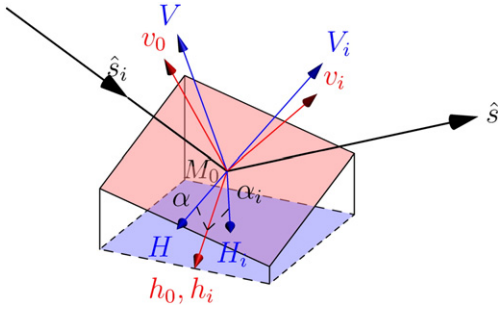
Eq. (1) ignores the correlation between surface points. Considering this correlation, the Smith illumination function has no closed-form expression since numerical integrations are involved. Consequently, $S_B^1$ with correlation cannot be expressed analytically. These integrations can be done numerically but require additional computing time. In this paper, it is assumed that the height autocorrelation function has a Gaussian form when the surface correlation is considered. The reader is referred to Bourlier, Saillard, and Berginc (2000a) for more details.

### 2.2. Rotation angle induced by 2D surfaces

For 2D rough surfaces, the orientations of the surface facets are arbitrary. As a result, the directions of the local horizontal and vertical polarizations, defined by the local normal $\hat{n}$ to the facet and the propagation direction of the incident ray $\hat{s}_i$ (denoted as $h_i$ and $v_i$) or that of the reflected ray $\hat{s}$ (denoted as $h$ and $v$), are different from one surface point to another.

To describe the polarization state of the sea surface reflectivity, global horizontal and vertical polarizations are introduced by the average sea surface (horizontal plane), or its normal — the zenith direction, and the propagation direction of the incident ray $\hat{s}_i$ or the reflected ray $\hat{s}$, denoted as $H_i$ and $V_i$, or $H$ and $V$, respectively.

Because of the arbitrariness of the local polarization directions, there is an angle $\alpha_i$ between $h_i$ and $H_i$, or equally between $v_i$ and $V_i$, if the facet is different from the horizontal plane. Similarly, there is an angle $\alpha$



**Fig. 1.** Single surface reflection and definitions of the different systems of coordinates $(x, y, z)$, $(X, Y, z)$ and $(X', Y', z)$.

**Fig. 2.** Single surface reflection by an arbitrary surface point $M_0$. There is a rotation angle $\alpha_i$ between the local polarization direction $h_i$ (or $v_i$) and the global one $H_i$ (or $V_i$). Similarly, there is a rotation angle $\alpha$ between $h_0$ (or $v_0$) and $H$ (or $V$).

between $h$ and $H$, or equally between $v$ and $V$, as illustrated in Fig. 2. In this case, one part of the incident energy in global $H_i$ (or $V_i$) polarization has to be projected into the local $v_i$ (or $h_i$) polarization by the angle $\alpha_i$. Similarly, one part of the reflected energy locally $h_i$ (or $v_i$) polarized has to be projected into the global $V$ (or $H$) polarization by the angle $\alpha$. In other words, cross polarizations occur. Cross polarizations never occur for 1D surfaces, because $\alpha_i$ and $\alpha$ always equal 0. The calculation of $\alpha$ and $\alpha_i$ is reported in Appendix A.

### 2.3. Determination of the reflectivity $\rho_1$

To derive the sea surface reflectivity, the local reflectivity of an arbitrary surface point $M_0$ is determined first, which is given by:

$$\rho_{h_0,v_0}(\chi_0) = |r_{h,v}(\chi_0)|^2, \tag{3}$$

where $r_{h,v}$ is the Fresnel reflection coefficients in local horizontal and vertical polarizations, respectively, and $\chi_0$ is the local angle of incidence at point $M_0$ (see Fig. 1 for definition).

Consider an incident ray, with components $I_{H_i}$ and $I_{V_i}$ in global $H_i$ and $V_i$ polarizations, which intersects the sea surface at a point $M_0$. If the tangent plane of $M_0$ is not identical to the average sea surface, there is an angle $\alpha_i$ between the polarization directions $H_i$ and $h_{0,i}$, or equally between $V_i$ and $v_{0,i}$. As a result, before performing the reflection, the intensity of the incident ray $\hat{s}_i$ in global $H_i$ and $V_i$ polarizations has to be projected into the local $h_{0,i}$ and $v_{0,i}$ polarization directions, as follows:

$$\begin{bmatrix} I_{h_{0,i}} \\ I_{v_{0,i}} \end{bmatrix} = \begin{bmatrix} \cos^2\alpha_i & \sin^2\alpha_i \\ \sin^2\alpha_i & \cos^2\alpha_i \end{bmatrix} \begin{bmatrix} I_{H_i} \\ I_{V_i} \end{bmatrix}, \tag{4}$$

where $\cos^2$ and $\sin^2$ stand for the projection of intensity.

After the surface reflection, the intensity of the reflected ray in local $h_0$ and $v_0$ is given by:

$$\begin{bmatrix} I_{h_0} \\ I_{v_0} \end{bmatrix} = \begin{bmatrix} \rho_{h_0} & 0 \\ 0 & \rho_{v_0} \end{bmatrix} \begin{bmatrix} I_{h_{0,i}} \\ I_{v_{0,i}} \end{bmatrix}. \tag{5}$$

As the local polarization directions are different from the global ones, the reflectivity in $h_0$ and $v_0$ polarizations is then projected to the global $H$ and $V$ polarization directions. The intensity of the reflected ray in global horizontal and vertical polarizations is then given by:

$$\begin{bmatrix} I_H \\ I_V \end{bmatrix} = \begin{bmatrix} \cos^2\alpha & \sin^2\alpha \\ \sin^2\alpha & \cos^2\alpha \end{bmatrix} \begin{bmatrix} I_{h_0} \\ I_{v_0} \end{bmatrix}. \tag{6}$$

By substituting Eqs. (4) and (5) into Eq. (6), the intensity of the reflected ray relates to that of the incident one as follows:

$$\begin{bmatrix} I_H \\ I_V \end{bmatrix} = \begin{bmatrix} \rho_{1,H_iH}^{\text{local}} & \rho_{1,V_iH}^{\text{local}} \\ \rho_{1,H_iV}^{\text{local}} & \rho_{1,V_iV}^{\text{local}} \end{bmatrix} \begin{bmatrix} I_{H_i} \\ I_{V_i} \end{bmatrix} \tag{7}$$

where

$$\begin{bmatrix} \rho_{1,H_iH}^{\text{local}} & \rho_{1,V_iH}^{\text{local}} \\ \rho_{1,H_iV}^{\text{local}} & \rho_{1,V_iV}^{\text{local}} \end{bmatrix} =$$
$$\begin{bmatrix} \cos^2\alpha & \sin^2\alpha \\ \sin^2\alpha & \cos^2\alpha \end{bmatrix} \begin{bmatrix} \rho_{h_0} & 0 \\ 0 & \rho_{v_0} \end{bmatrix} \begin{bmatrix} \cos^2\alpha_i & \sin^2\alpha_i \\ \sin^2\alpha_i & \cos^2\alpha_i \end{bmatrix}. \tag{8}$$

The terms $\rho_{1,V_iH}^{\text{local}}$ and $\rho_{1,H_iV}^{\text{local}}$ represent the reflectivity with global cross polarizations ($V_i \to H$ or $H_i \to V$). In the terms $\rho_{1,H_iH}^{\text{local}}$ and $\rho_{1,V_iV}^{\text{local}}$, no global cross polarization occurs. However, local cross polarizations ($H_i \to v_i$, $V_i \to h_i$, $h_0 \to V$, and $v_0 \to H$) still take place, with each $\sin^2\alpha$ or $\sin^2\alpha_i$ standing for one local cross polarization.

The bidirectional reflectivity with one surface reflection of a rough sea surface is obtained by averaging the local reflectivity over the whole surface, given by (Bourlier et al., 2001):

$$\rho_{1,A,B}(\theta,\phi,\theta_i,\phi_i) = \left\langle \rho_{1,A,B}^{\text{local}} g_0 S_B^1 \right\rangle_1, \tag{9}$$

where $A = \{H_i,V_i\}$ and $B = \{H,V\}$. The term $g_0$ results from projecting the area of the facet $M_0$ into the direction perpendicular to the observation direction $\hat{s}$, given by (Bourlier et al., 2001):

$$g_0 = 1 - \left(\gamma_{x_0}\cos\phi + \gamma_{y_0}\sin\phi\right)\tan\theta. \tag{10}$$

where $S_B^1$ is the bistatic illumination function given by Eq. (1). The symbol $\langle\cdots\rangle_1$ stands for the statistical average over the slopes of an arbitrary surface point, given by:

$$\langle\cdots\rangle_1 = \int_{-\infty}^{+\infty}\int_{-\infty}^{+\infty} \cdots p\left(\gamma_{x_0},\gamma_{y_0}\right) d\gamma_{x_0} d\gamma_{y_0}, \tag{11}$$

where $p\left(\gamma_{x_0},\gamma_{y_0}\right)$ is the surface slope PDF. Eq. (11) involves integrations over two Dirac delta functions. See Appendix B for the details of the calculation.

The hemispherical reflectivity with one reflection is obtained by integrating the bidirectional one on the incidence direction $\hat{s}_i(\theta_i,\phi_i)$ (or observation direction $\hat{s}(\theta,\phi)$) over the upper hemisphere, as follows:

$$\rho_{1,A,B}^{\text{hemi}}(\theta,\phi) = \int_0^{2\pi}\int_0^{\pi/2} \rho_{1,A,B}(\theta,\phi,\theta_i,\phi_i) d\theta_i d\phi_i, \tag{12}$$

where $\rho_{1,A,B}$ is the bidirectional reflectivity.

### 3. Reflectivity with two reflections

The sea surface reflectivity with two reflections corresponds to the radiance from the sky reflected twice by the sea surface. Fig. 3 illustrates two successive reflections by the surface.

A new system of coordinates $(X'',Y'',z)$ is defined according to the direction of the incident ray $\hat{s}_i(\theta_2,\phi_2)$, by rotating the $(x,y)$ basis anticlockwise through an angle $\phi_2$ so that $\hat{s}_i$ belongs to the $(X'',z)$ plane. The system of coordinates $(X',Y',z)$ is then defined according to the reflected ray $\hat{s}'$ of $\hat{s}_i$, and $(X,Y,z)$ is always defined according to the observation direction $\hat{s}$, similar to that in Fig. 1.
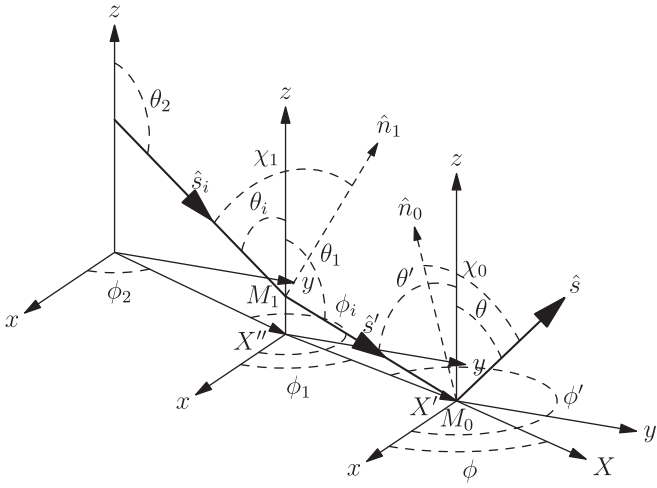
**Fig. 3.** Two successive surface reflections by two surface points $M_1$ and $M_0$, and the definition of the new system of coordinates $(X'', Y'', z)$.

### 3.1. $S_B$ with two surface reflections

To take into account the influence of double surface reflections, a bistatic illumination function with two reflections $S_B^2$ must be employed to evaluate the occurrence that the incident ray is reflected twice by the surface. This article adopts the model developed by Li et al. (2013) for 1D surfaces and extends it to 2D surfaces.

Following Li et al. (2013), four events are defined as:

- "the ray $M_0(\hat{s})$ does not intersect the surface" is denoted as $a$;
- "the reflected ray $M_0(\hat{s}'^{-})$ of $M_0(\hat{s}^{-})$ intersects the surface" is denoted as $b$;
- "the reflected ray of $M_0(\hat{s}'^{-})$ propagates in the $\hat{s}_i^{-}$ direction" is denoted as $c$;
- "the ray $M_1(\hat{s}_i^{-})$ does not intersect the surface" is denoted as $d$.

The bistatic illumination function $S_B^2$ is then given by (Li et al., 2013):

$$S_B^2 = p(abcd) = p(ab)p(c|ab)p(d|abc). \tag{13}$$

#### 3.1.1. Determination of $p(ab)$

The first part $p(ab)$ equals exactly the monostatic illumination function with one surface reflection (Li, Pinel, & Bourlier, 2012; Li et al., 2011; Masuda, 2006; Wu & Smith, 1997). This article employs the model of Li et al. (2012). Ignoring the correlation between the surface points, it is given by:

$$p(ab) = \Upsilon\left(\mu - \gamma_{x_0}\right)$$
$$\times \begin{cases} \dfrac{1}{1 + \Lambda(\mu)} & \text{if } \theta' > 90° \\[2mm] \dfrac{\Lambda^{-}(\mu_1)}{[1 + \Lambda(\mu)][1 + \Lambda(\mu) + \Lambda^{-}(\mu_1)]} & \text{if } \theta' < 90° \end{cases}, \tag{14}$$

where $\mu_1 = \cot\theta_1$ is the slope of the ray $\hat{s}'$. Here, the calculation of $p(ab)$ is based on the Smith illumination function. As we mentioned previously, there is no closed-form expression for the Smith illumination function after considering the correlation between surface points. The reader is referred to Li et al. (2011) for more details.

#### 3.1.2. Determination of $p(c|ab)$

The conditional probability $p(c|ab)$ corresponds to the probability that the reflected ray of $M_0(\hat{s}'^{-})$ propagates along the $\hat{s}_i^{-}$ direction. It is expressed by Dirac delta functions, as follows (Li et al., 2013):

$$p(c|ab) = \delta\left(\theta_i^{\text{spe}} - \theta_i\right)\delta\left(\phi_i^{\text{spe}} - \phi_i\right), \tag{15}$$

where $\theta_i^{\text{spe}}$ and $\phi_i^{\text{spe}}$ are the zenith and azimuth angles of the specular reflection direction $\hat{s}_i^{-,\text{spe}}$ of $\hat{s}'^{-}$ by the point $M_1$.

#### 3.1.3. Determination of $p(d|abc)$

The conditional probability $p(d|abc)$ corresponds to the probability that $M_1$ is seen by the emitter along $\hat{s}_i^{-}$ given the event $abc$. As no obvious relation can be obtained between $d$ and $abc$, it is assumed that they are independent (Li et al., 2013). In this case, $p(d|abc)$ is expressed approximately by the Smith illumination function, given by:

$$p(d|abc) \approx p(d) = \frac{1}{1 + \Lambda^{-}(\mu_i)}, \tag{16}$$

where $\mu_i = -\cot\theta_i$ is the slope of the incidence direction in the $(X'', z)$ plane.

The statistical bistatic illumination function with two reflections $S_B^2$ is obtained by substituting Eqs. (14), (15) and (16) into Eq. (13). The average bistatic illumination function with two reflections $\overline{S}_B^2$ is obtained by averaging $S_B^2$ over the slopes of the surface, expressed as:

$$\overline{S}_B^2(\theta, \phi, \theta_i, \phi_i) = \left\langle S_B^2 \right\rangle_2, \tag{17}$$

where $\langle \cdots \rangle_2$ stands for the statistical average over the slopes of two arbitrary surface points, given by:

$$\langle \cdots \rangle_2 = \int_{-\infty}^{+\infty} \int_{-\infty}^{+\infty} \int_{-\infty}^{+\infty} \int_{-\infty}^{+\infty} \cdots$$
$$p\left(\gamma_{x_0}, \gamma_{y_0}, \gamma_{x_1}, \gamma_{y_1}\right) d\gamma_{x_1} d\gamma_{y_1} d\gamma_{x_0} d\gamma_{y_0}, \tag{18}$$

with $p\left(\gamma_{x_0}, \gamma_{y_0}, \gamma_{x_1}, \gamma_{y_1}\right)$ being the joint PDF of the slopes of the two surface points $M_0$ and $M_1$. In this article, it is assumed that the slopes of $M_0$ and $M_1$ are uncorrelated. This is because the distance between $M_0$ and $M_1$ is unknown analytically, which makes it impossible to evaluate the correlation.

The hemispherical bistatic illumination function with two reflections is obtained by integrating $\overline{S}_B^2$ on the incidence direction $\hat{s}_i(\theta_i, \phi_i)$ (or the observation direction $\hat{s}(\theta, \phi)$) over the upper hemisphere, given by:

$$\overline{S}_B^{2,\text{hemi}}(\theta, \phi) = \int_0^{2\pi} \int_0^{\pi/2} \overline{S}_B^2(\theta, \phi, \theta_i, \phi_i) d\theta_i d\phi_i. \tag{19}$$
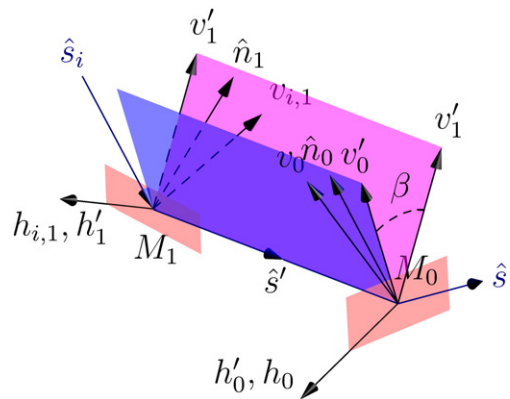


**Fig. 4.** The incident ray $\hat{s}_i$ is reflected by the point $M_1$ and then by $M_0$ into the observation direction $\hat{s}$. A rotation angle $\beta$ occurs between the local polarization directions of $M_1$ and $M_0$.

### 3.2. Rotation angle introduced by 2D surfaces

The local horizontal and vertical polarization directions of the point $M_1$ defined by the incident ray $\hat{s}_i$ and its local normal $\hat{n}_1$ are denoted as $h_{1,i}$ and $v_{1,i}$, respectively. As discussed in Section 2.2, there is a rotation angle $\alpha_i$ between $H_i$ and $h_{1,i}$, or between $V_i$ and $v_{1,i}$ if the facet $M_1$ is different from the average sea surface (horizontal surface). Similarly, for the point $M_0$, there is a rotation angle $\alpha$ between $h_0$ and $H$, or between $v_0$ and $V$.

Besides, as the facets $M_1$ and $M_0$ are usually not parallel, there is another rotation angle $\beta$ between the local polarization directions of the point $M_1$ (defined by $\hat{n}_1$ and $\hat{s}'$, denoted as $h_1'$ and $v_1'$) and those of $M_0$ (defined by $\hat{n}_0$ and $\hat{s}'$, denoted as $h_0'$ and $v_0'$), as illustrated in Fig. 4. Cross polarizations occur as long as the local planes of incidence of $M_0$ and $M_1$ are not identical. See Appendix B of Li et al. (2012) for the calculation of $\beta$. For 1D surfaces, these two planes are always identical ($\beta = 0°$), thus cross polarizations do not occur.

### 3.3. Determination of reflectivity $\rho_2$

To derive the surface reflectivity with two reflections, the local reflectivity with two surface reflections is derived first. The local reflectivity of $M_1$ with one reflection is given by:

$$\rho_{1,h,v}(\chi_1) = |r_{h,v}(\chi_1)|^2, \tag{20}$$

where $r_{h,v}$ is the Fresnel reflection coefficients in local horizontal and vertical polarizations, respectively, and $\chi_1$ is the local angle of incidence.

Similarly as in Section 2.3, an incident ray with intensity $I_{H_i}$ and $I_{V_i}$ in global $H_i$ and $V_i$ polarizations is considered. As discussed previously, there is an angle $\alpha_i$ between $H_i$ (or $V_i$) and $h_{1,i}$ (or $v_{1,i}$) at point $M_1$. The intensity of the incident ray in local $h_{1,i}$ and $v_{1,i}$ polarizations is given by:

$$\begin{bmatrix} I_{h_{1,i}} \\ I_{v_{1,i}} \end{bmatrix} = \begin{bmatrix} cos^2\alpha_i & sin^2\alpha_i \\ sin^2\alpha_i & cos^2\alpha_i \end{bmatrix} \begin{bmatrix} I_{H_i} \\ I_{V_i} \end{bmatrix}. \tag{21}$$

After the surface reflection by $M_1$, the intensity of the reflected ray $\hat{s}'$ in local $h_1'$ and $v_1'$ is given by:

$$\begin{bmatrix} I_{h_1'} \\ I_{v_1'} \end{bmatrix} = \begin{bmatrix} \rho_{h_1} & 0 \\ 0 & \rho_{v_1} \end{bmatrix} \begin{bmatrix} I_{h_{1,i}} \\ I_{v_{1,i}} \end{bmatrix}. \tag{22}$$

As the orientations of the facets $M_1$ and $M_0$ are different, there is usually an angle $\beta$ between the local polarization directions of $M_0$ and $M_1$. The projection of the intensity of the ray $\hat{s}'$ in $h_1'$ and $v_1'$ polarizations into $h_0'$ and $v_0'$ polarizations is expressed by:

$$\begin{bmatrix} I_{h_0'} \\ I_{v_0'} \end{bmatrix} = \begin{bmatrix} cos^2\beta & sin^2\beta \\ sin^2\beta & cos^2\beta \end{bmatrix} \begin{bmatrix} I_{h_1'} \\ I_{v_1'} \end{bmatrix}. \tag{23}$$

After the surface reflection by $M_0$, the intensity of the reflected ray in local $h_0$ and $v_0$ is given by:

$$\begin{bmatrix} I_{h_0} \\ I_{v_0} \end{bmatrix} = \begin{bmatrix} \rho_{h_0} & 0 \\ 0 & \rho_{v_0} \end{bmatrix} \begin{bmatrix} I_{h_0'} \\ I_{v_0'} \end{bmatrix}. \tag{24}$$

The projection of the intensity of the ray $\hat{s}$ in local $h_0$ and $v_0$ polarizations into global $H$ and $V$ polarizations is expressed in Eq. (6). By substituting Eqs. (21)–(24) for Eq. (6), the intensity of the reflected ray relates to that of the incident one as:

$$\begin{bmatrix} I_H \\ I_V \end{bmatrix} = \begin{bmatrix} \rho_{2,H_iH}^{local} & \rho_{2,V_iH}^{local} \\ \rho_{2,H_iV}^{local} & \rho_{2,V_iV}^{local} \end{bmatrix} \begin{bmatrix} I_{H_i} \\ I_{V_i} \end{bmatrix} \tag{25}$$

where

$$\begin{bmatrix} \rho_{2,H_iH}^{local} & \rho_{2,V_iH}^{local} \\ \rho_{2,H_iV}^{local} & \rho_{2,V_iV}^{local} \end{bmatrix} = \begin{bmatrix} cos^2\alpha & sin^2\alpha \\ sin^2\alpha & cos^2\alpha \end{bmatrix} \begin{bmatrix} \rho_{h_0} & 0 \\ 0 & \rho_{v_0} \end{bmatrix} \begin{bmatrix} cos^2\beta & sin^2\beta \\ sin^2\beta & cos^2\beta \end{bmatrix}$$
$$\begin{bmatrix} \rho_{h_1} & 0 \\ 0 & \rho_{v_1} \end{bmatrix} \begin{bmatrix} cos^2\alpha_i & sin^2\alpha_i \\ sin^2\alpha_i & cos^2\alpha_i \end{bmatrix}. \tag{26}$$

The sea surface bidirectional reflectivity with two reflections is obtained by averaging the local ones over the whole surface, as follows (Li et al., 2013):

$$\rho_{2,A,B}(\theta, \phi, \theta_i, \phi_i) = \left\langle \rho_{2,A,B}^{local} g_0 S_B^2 \right\rangle_2, \tag{27}$$

where $S_B^2$ is the bistatic illumination function with two surface reflections given by Eq. (13).

The hemispherical reflectivity with two reflections is obtained by integrating the bidirectional one on the incidence direction $\hat{s}_i(\theta_i, \phi_i)$ (or the observation direction $\hat{s}(\theta, \phi)$) over the upper hemisphere, as follows:

$$\rho_{2,A,B}^{hemi}(\theta, \phi) = \int_0^{2\pi} \int_0^{\pi/2} \rho_{2,A,B}(\theta, \phi, \theta_i, \phi_i) d\theta_i d\phi_i, \tag{28}$$

where $\rho_{2,A,B}$ is the bidirectional reflectivity with two reflections.

To calculate the integrations in Eqs. (18) and (27), the changes of variables from $d\gamma_{x_1} d\gamma_{y_1}$ to $d\theta_i^{spe} d\phi_i^{spe}$ are performed as shown in Appendix B, by replacing $\hat{s}$ with $\hat{s}'$ and $\hat{n}_0$ with $\hat{n}_1$. Besides, the following ones are also performed:

$$\begin{aligned} \gamma_{x_1} &= \gamma_{X_1'} cos\phi_1 - \gamma_{Y_1'} sin\phi_1, \\ \gamma_{y_1} &= \gamma_{X_1'} sin\phi_1 + \gamma_{Y_1'} cos\phi_1, \end{aligned} \tag{29}$$

where $\gamma_{X_1'}$ and $\gamma_{Y_1'}$ are the slopes of the point $M_1$ in the $X'$ and $Y'$ directions, respectively. The integration variables in Eq. (18) become:

$$d\gamma_{x_1} d\gamma_{y_1} d\gamma_{x_0} d\gamma_{y_0} = J d\gamma_{X_1'} d\gamma_{Y_1'} d\gamma_{X_0} d\gamma_{Y_0}, \tag{30}$$

with the Jacobian $J = 1$.

## 4. Numerical results

### 4.1. Parameters used in the calculations

In this article, it is assumed that the sea surface slope PDF $p_y$ is Gaussian with zero mean. The sea surface root mean square (RMS) slopes in the up-wind and cross-wind are given by the model of Cox and Munk (1954). Under such an assumption, the surface slopes along any horizontal direction are also Gaussian with zero mean. The reader is referred to Eq. (31) of Bourlier et al. (2000a) for the derivation of the RMS slope along an arbitrary direction.

The integrations in Eq. (18) require the knowledge of the slope PDF of point $M_1$. Given that $M_1$ is the intersection of the ray $\hat{s}'^-$ (inverse path), its PDF is different from that of the whole sea surface. Following the discussion in Li et al. (2012), the slope PDF is given by:

$$p_{\gamma_1}\left(\gamma_{X_1'}, \gamma_{Y_1'}\right) = \frac{\Upsilon\left(\mu_1 - \gamma_{X_1'}\right)}{\int_{-\infty}^{\mu_1} p_\gamma\left(\gamma_{X_1'}\right) d\gamma_{X_1'}} p_\gamma\left(\gamma_{X_1'}\right) p_\gamma\left(\gamma_{Y_1'}\right), \tag{31}$$

where $\gamma_{X_1'}$ and $\gamma_{Y_1'}$ are the slopes of $M_1$ along the $X'$ and $Y'$ directions, respectively.
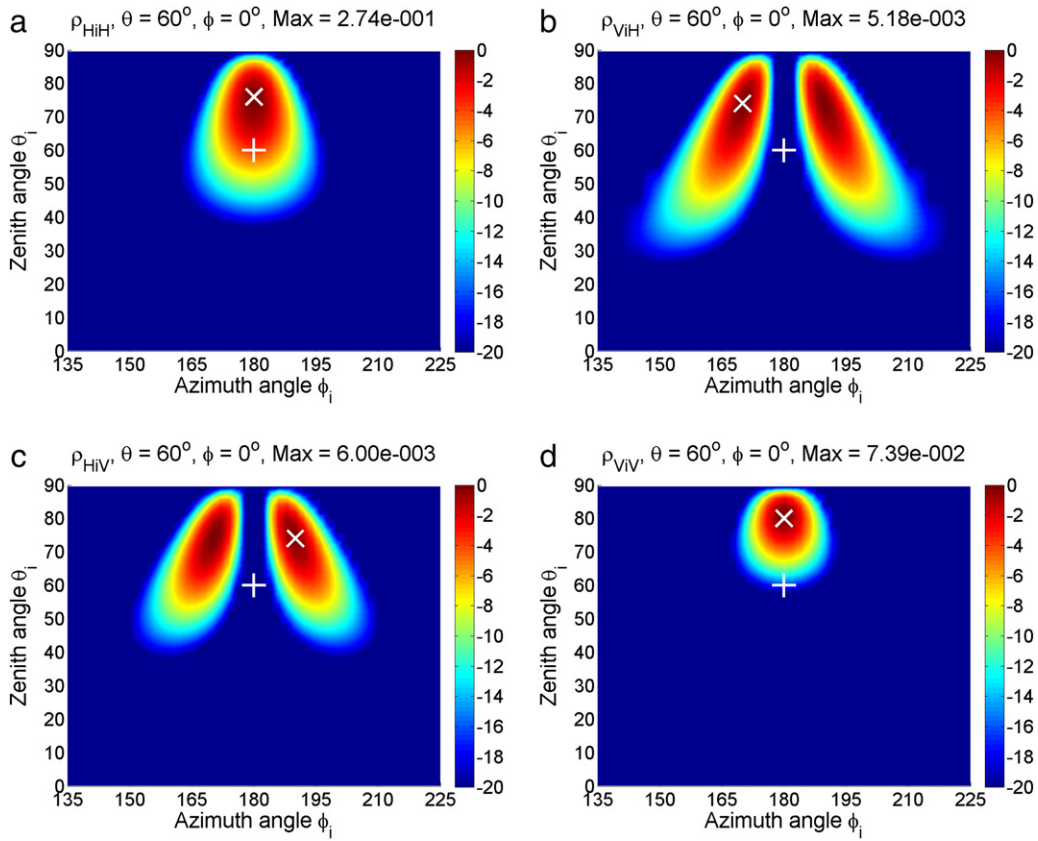
**Fig. 5.** Normalized bidirectional reflectivity with one surface reflection is shown in dB scale, in (a) $H_iH$, (b) $V_iH$, (c) $H_iV$ and (d) $V_iV$ polarizations. The sensor is located in the direction $\hat{s} = \{\theta = 60°, \phi = 0°\}$. The wind speed is $u_{12} = 10$ m/s, and the wavelength is $\lambda = 10$ μm. The symbol "+" represents the global reflection direction, and the symbol "×" represents the maximum of the reflectivity.
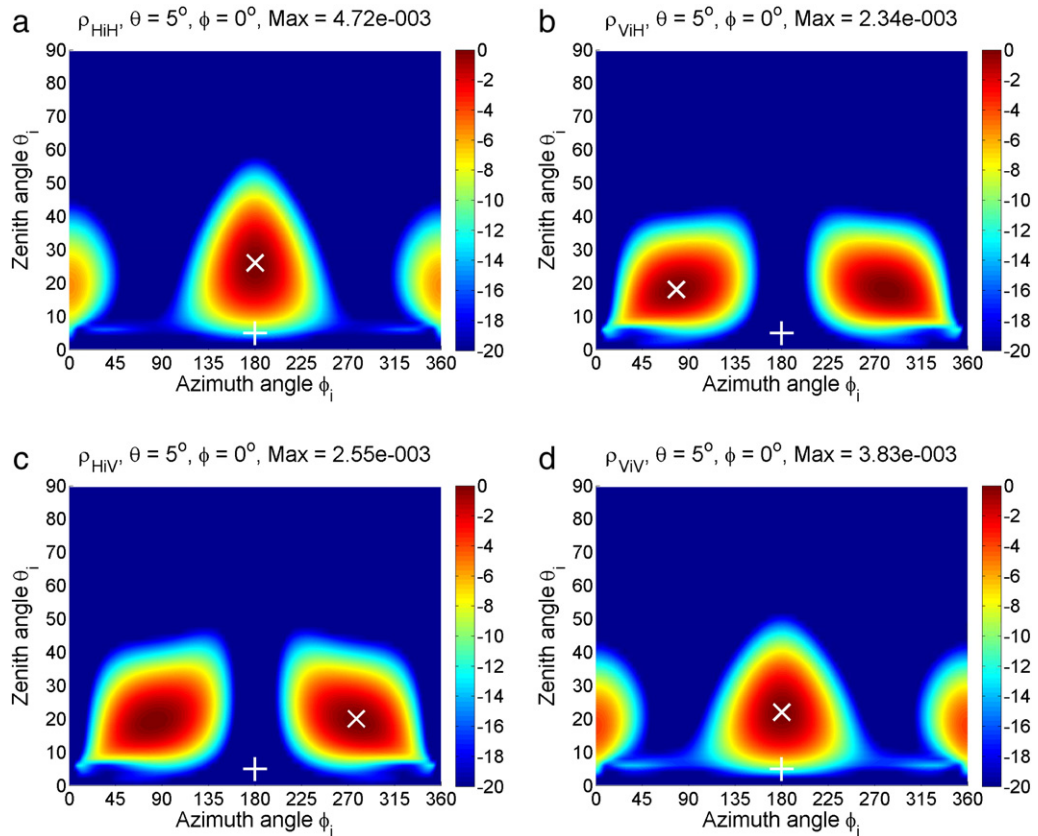


**Fig. 6.** Normalized bidirectional reflectivity for the same parameters as Fig. 5, except that the sensor is located in the direction $\hat{s} = \{\theta = 5°, \phi = 0°\}$.

The infrared wavelength in the infrared atmospheric windows of 3–5 μm and 8–13 μm is considered in this article. The sea water refractive index $n$ in this region is given by the model of Hale and Querry (1973).

### 4.2. Reflectivity with one reflection $\rho_1$

#### 4.2.1. Bidirectional reflectivity $\rho_1$

The bidirectional reflectivity with one surface reflection $\rho_1$ is given by Eq. (9). The results of $\rho_{1,H_iH}$, $\rho_{1,H_iV}$, $\rho_{1,V_iH}$ and $\rho_{1,V_iV}$ are shown in Figs. 5 and 6, for a wind speed at 12.5 m above the sea surface $u_{12} = 10$ m/s (Beaufort scale ≈ 5) and for an infrared wavelength $\lambda = 0$ μm. In this paper, the bidirectional reflectivities $\rho_1$ and $\rho_2$ are always presented versus the zenith and azimuth angles of the emitter, whereas the position of the sensor is fixed, because the inverse path is used in the determination of the bistatic illumination functions. The sensor is located in $\hat{s} = \{\theta = 60°, \phi = 0°\}$ in Fig. 5 and in $\hat{s} = \{\theta = 5°, \phi = 0°\}$ in Fig. 6. The results are normalized by the corresponding maximum and are shown in decibel (dB) for better clarity in the figure as $\rho_1$ is very small in comparison to unity, which is expressed as:

$$\rho = 10\log_{10}(\rho/max(\rho)). \tag{32}$$

The value of the maximum is given in the title of each subfigure. The results without considering the correlation between surface points are shown. The results with the correlation are calculated but they are not shown as they are very similar to the uncorrelated ones.

The global reflection direction of $\hat{s}^-$ is denoted as "+" (here $\hat{s}_i^- = \{\theta_i = 60°, \phi_i = 180°\}$ in Fig. 5, and $\hat{s}_i^- = \{\theta_i = 5°, \phi_i = 180°\}$ in Fig. 6), and the position of the maximum of $\rho_1$ is noted as "×". It is shown that the maximum of the bidirectional reflectivity $\rho_1$ is shifted toward the horizon ($\theta_i \approx \{76°, 74°, 74°, 80°\}$ in Fig. 5, $\theta_i \approx \{26°, 18°, 20°, 22°\}$ in Fig. 6, for $\rho_1$ in $H_iH$, $V_iH$, $H_iV$ and $V_iV$ polarizations, respectively), which is also reported by Ross et al. (2005) and Su, C., and R. (2002) when deriving the sun glitter on the sea surfaces.

It is notable that the cross-polarization terms ($\rho_{1,V_iH}$ in Figs. 5b and 6b, and $\rho_{1,H_iV}$ in Figs. 5c and 6c) equal zero along the horizontal projection direction of the global specular reflection direction (where $\phi_i = \phi + 180°$). Along this direction, the sensor (thus $\hat{s}$) is located in the global plane of incidence defined by the incidence direction $\hat{s}_i$ and the zenith. This configuration can be treated as considering a one-dimensional (1D) surface, thus cross polarization never occurs (Li et al., 2013).

Besides, the bidirectional reflectivity $\rho_1$ is symmetrical about the global plane of incidence (which corresponds to the $\phi_i = \phi + 180°$ direction) when the sensor is located in the up-wind direction $\phi = 0°$. Similar simulations are performed for other observation directions. The same conclusion is found for sensors located in the down- and cross-wind directions, because of the symmetry of the sea surface about these directions. However, apart from these directions, the bidirectional reflectivity $\rho_1$ is no longer symmetrical about the global plane of incidence.

In Fig. 5, the terms $\rho_{1,H_iH}$ and $\rho_{1,V_iV}$ (maxima of the order of $10^{-1}$) are more significant than the cross polarization terms $\rho_{1,H_iV}$ and $\rho_{V_iH}$ (maxima of the order of $10^{-3}$), meaning that the cross polarization effect is weak for this observation direction $\hat{s}$. The reason is that, the average rotation angles $\alpha$ and $\alpha_i$ are very small for $\hat{s}$ with large zenith observation angles $\theta$. Consequently, $\sin^2\alpha$ and $\sin^2\alpha_i$ in Eq. (8) are small, leading to a weak cross-polarized reflectivity.

In Fig. 6, $\rho_{1,H_iH}$ and $\rho_{1,V_iV}$ are much smaller than the ones in Fig. 5. On the other hand, the terms $\rho_{1,H_iV}$ and $\rho_{1,V_iH}$ in Fig. 6 are comparable in level to the co-polarized ones $\rho_{1,H_iH}$ and $\rho_{1,V_iV}$, with maxima of $10^{-3}$. The reason is that, firstly, the local angles of incidence are small (with mean value about 5°), which means that the Fresnel reflection coefficients in horizontal $r_h$ and vertical $r_v$ polarizations are comparable; secondly, the mean values of the rotation angles $\alpha$ and $\alpha_i$ are close to 45° (similar to that in Fig. 5b in Li et al., 2012), leading to the fact that $\sin^2\alpha$, $\cos^2\alpha$, $\sin^2\alpha_i$ and $\cos^2\alpha_i$ are comparable.
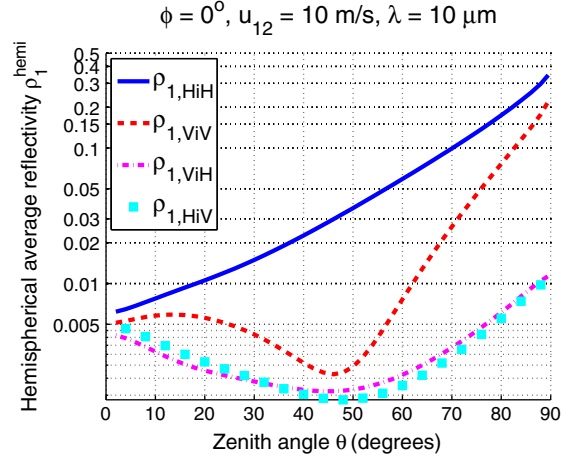


**Fig. 7.** Hemispherical reflectivity with one surface reflection versus the zenith angle $\theta$. The sensor is located in the up-wind direction $\phi = 0°$. The wind speed is $u_{12} = 10$ m/s, and the wavelength is $\lambda = 10$ μm.

It is also notable that, for $\rho_{1,H_iH}$ and $\rho_{1,V_iV}$, one part of the incident energy is reflected "back" toward the sensor (along $\phi_i = 0°$ or $\phi_i = 360°$), which was not observed in Fig. 5. The reason is that the slope required for a "back-scattering" is smaller in absolute value and is easier to achieve when the sensor (or the emitter) is closer to the zenith.

#### 4.2.2. Hemispherical reflectivity $\rho_1^{hemi}$

The hemispherical reflectivity with one reflection $\rho_1^{hemi}$ is given by Eq. (12). The results without considering the correlation between surface points are shown in Fig. 7 versus the zenith angle $\theta$ in the up-wind direction $\phi = 0$, for a wind speed $u_{12} = 10$ m/s and for an infrared wavelength $\lambda = 10$ μm. Note that the $y$ axis is in $log$ scale. The results with correlation are not shown because no significant difference with the uncorrelated ones is found.

It is shown that the cross-polarization terms ($\rho_{1,H_iV}$ and $\rho_{1,V_iH}$) are always near zero. They are relatively significant when the zenith angles are very small or very large ($\theta < 10°$ or $\theta > 80°$). The terms $\rho_{1,H_iH}$ and $\rho_{1,V_iV}$ are always dominant, with $\rho_{1,H_iH}$ being larger. Note that $\rho_1^{hemi}$ in cross- and in co-polarizations is comparable in level for $\theta$ near 0°, which is predicted in Fig. 6.

The influence of the Brewster angle is clearly observed in the reflectivity in $H_iV$, $V_iH$ and $V_iV$ polarizations. It is notable that the pseudo-Brewster angle here ($\theta_{pB} = \{48°, 46°, 46°\}$ for $\rho_1$ in $H_iV$, $V_iH$ and $V_iV$ polarizations) is shifted toward small $\theta$ with respect to that of a flat surface ($\theta_B = 50.6°$), which is also reported by Leskova, Maradudin, and Novikov (2000) for the case in which a wave propagates from a media with smaller permittivity toward one with larger permittivity.

### 4.3. Reflectivity $\rho_2$ with two reflections

#### 4.3.1. Bistatic illumination function $S_B^2$

The average bistatic illumination function with two reflections $\bar{S}_B^2$ is given by Eq. (17). The results of $\bar{S}_B^2$ are normalized and shown in Fig. 8(a) in dB scale (see Eq. (32)), for a wind speed $u_{12} = 10$ m/s. The sensor is in the direction $\hat{s} = \{\theta = 60°, \phi = 0°\}$.

The results without considering the correlation between surface points are shown. The ones with correlation have a similar form but are slightly smaller in level. It is shown that $\bar{S}_B^2$ is significant only around the global plane of incidence (here the direction $\phi_i = 180°$). Beyond this direction, $\bar{S}_B^2$ decreases rapidly to zero. Similar to the reflectivity with one reflection, the peak of $\bar{S}_B^2$ (noted as ×) is also shifted toward the horizon compared to the global reflection direction (noted as +).

The hemispherical bistatic illumination function with two reflections $\bar{S}_B^{2,hemi}$ is given by Eq. (19). The results with and without
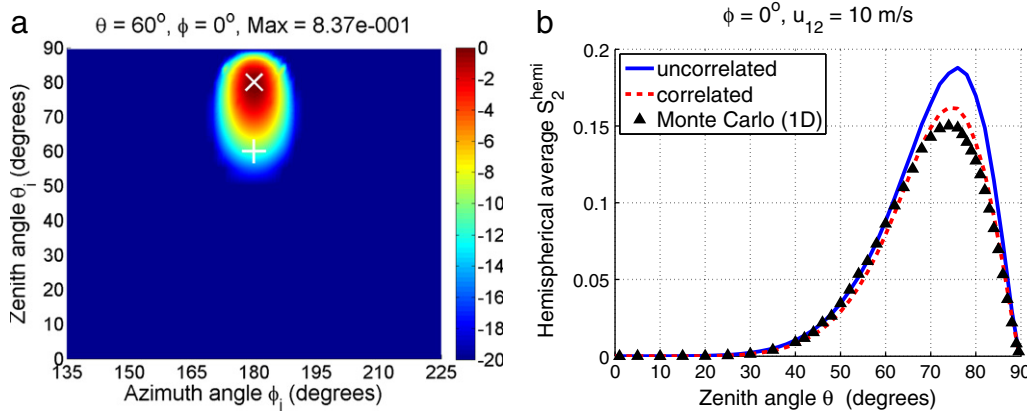
**Fig. 8.** Normalized bistatic illumination function with two surface reflections is shown in dB (a). The hemispherical bistatic illumination function is shown along the up-wind direction (b).

considering the surface correlation are shown in Fig. 8(b), for a wind speed $u_{12} = 10$ m/s along the up-wind direction $\phi = 0°$. It is shown that double surface reflections are negligible for small zenith angles $\theta < 40°$, which may concern the satellite applications. Nevertheless, they become significant for larger zenith angles. Maxima about 0.2 are found around $\theta = 75°$, meaning that about 20% of the incident rays along this $\hat{s}^-$ (inverse path) undergo double surface reflections before they leave the surface.

The results are compared with those obtained by a Monte Carlo ray tracing method Li et al. (2013). Although this Monte Carlo ray tracing algorithm is performed for 1D surfaces, it reflects the general level and the form of $\bar{S}_B^{2,hemi}$, thus it is comparable with the 2D surface model here. Very similar conclusions to the ones obtained by Li et al. (2013) with the 1D surface model are found. It is shown that the model with

correlation better agrees with the Monte Carlo ray tracing method. Neglecting the correlation leads to an overestimation for $65° < \theta < 89°$.

### 4.3.2. Bidirectional reflectivity $\rho_2$

The bidirectional reflectivity with two reflections $\rho_2$ is given by Eq. (27). The results of $\rho_{2,H_iH}$, $\rho_{2,H_iV}$, $\rho_{2,V_iH}$ and $\rho_{2,V_iV}$ are shown in Fig. 9, for the same parameters as in Fig. 5. The results are normalized by the maximum and are shown in dB scale, as expressed by Eq. (32). The results for the same parameters as in Fig. 6 are not shown, as they are too small in level (maxima of the order of $10^{-7}$).

As expected from Fig. 8(a), for a given incidence direction $\hat{s}^-$ (inverse path), the bidirectional reflectivity with two reflections $\rho_2$ is significant for $\hat{s}_i$ with large $\theta_i$ and around the horizontal direction of the global reflection direction (here the direction $\phi_i = 180°$). Shifts of
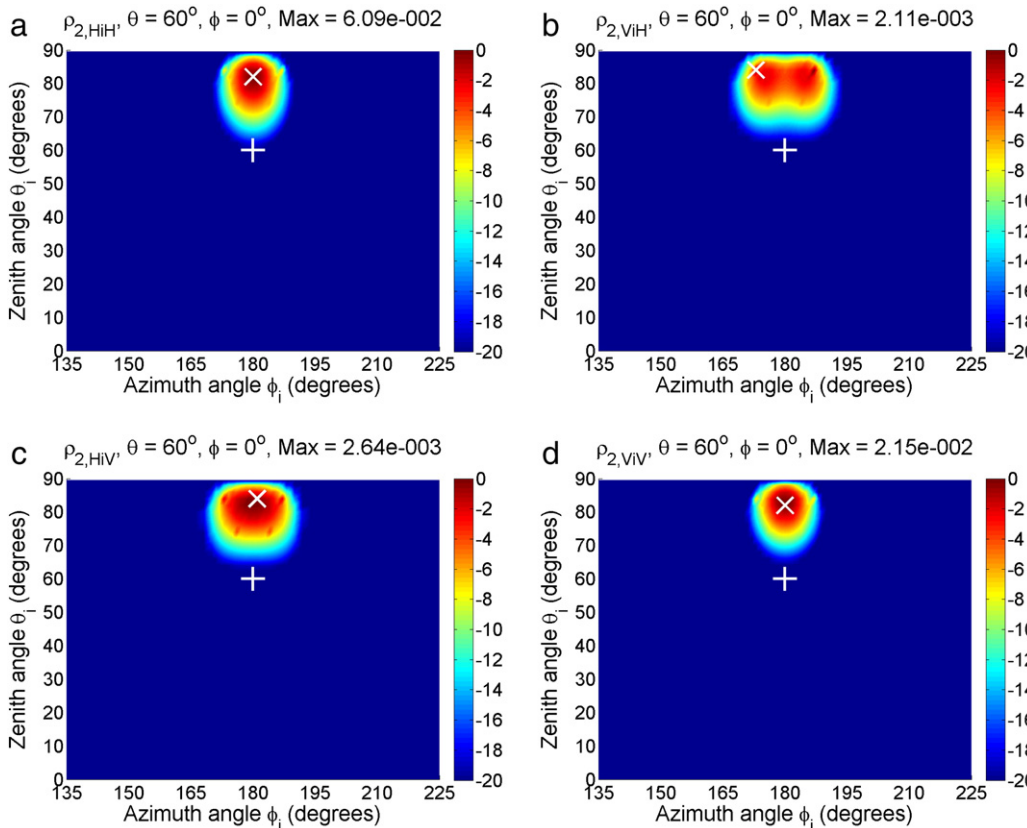


**Fig. 9.** Normalized bidirectional reflectivity with two surface reflections is shown in dB scale for the same parameters as in Fig. 5.

maxima (noted as ×) toward the horizon are also found for all polarizations with respect to the global specular reflection direction (noted as +).

The peaks of $\rho_2$ in $H_iH$ (Fig. 9a) and $V_iV$ (Fig. 9d) polarizations are found in the horizontal direction of the global reflection direction, whereas the peaks of $\rho_2$ in $V_iH$ (Fig. 9b) and $H_iV$ (Fig. 9c) polarizations are shifted beside this direction, which is also observed in $\rho_1$ (see Fig. 5). However, unlike $\rho_1$, $\rho_2$ in $V_iH$ and $H_iV$ polarizations is not zero in the horizontal direction of the global reflection direction. The reason is that, although $\hat{s}_i$ is parallel to the plane defined by $\hat{s}$ and the zenith, $M_1$ can still be outside of this plane. In other words, the incidence and observation planes are parallel but may not be identical and the surface cannot be treated as 1D. Thus, cross-polarizations can still occur.

The reflectivity $\rho_2$ in $V_iH$ and $H_iV$ polarizations, with maxima of the order of $10^{-3}$, is much smaller than that in $H_iH$ and $V_iV$ polarizations which have maxima of the order of $10^{-2}$. Note that this conclusion is also obtained in the reflectivity with one reflection $\rho_1$ for $\hat{s}$ with large $\theta$ (see Fig. 5). Besides, $\rho_2$ in $H_iH$ and $V_iV$ polarizations is more significant than $\rho_1$ in $H_iV$ and $V_iH$ polarizations (maxima of the order of $10^{-3}$). Thus, it can be concluded that, in terms of level, it is more important to take into account the second reflection than the cross-polarization terms.

### 4.3.3. Hemispherical reflectivity $\rho_2^{hemi}$

The hemispherical reflectivity with two reflections $\rho_2^{hemi}$ is given by Eq. (28). The results without considering the correlation between surface points are shown in Fig. 10 versus the zenith angle $\theta$ in the up-wind direction $\phi = 0$, for the same parameters as in Fig. 7. The results with correlation are not shown as they are similar to the ones without correlation, except that they are smaller in level for $65° < \theta < 89°$, which is also predicted in Fig. 8(b).

The hemispherical reflectivity with two reflections $\rho_2^{hemi}$ in $H_iH$ and $V_iV$ polarizations is significant for large $\theta$, with maxima of about 0.02 and 0.012, respectively, around $\theta = 80°$, meaning that about 2% and 1.2% of the incident energy along $\hat{s}^- (\theta = 80°, \phi = 0°)$ undergo double surface reflections.

On the other hand, $\rho_2^{hemi}$ in $V_iH$ and $H_iV$ is much smaller. They are relatively significant for large $\theta$ ($\theta > 60°$), which is also true for the hemispherical reflectivity with one reflection $\rho_1^{hemi}$ (see Fig. 7). Maxima are reached around $\theta = 80°$, but are much smaller in level ($< 1.5 \times 10^{-3}$) than the ones in $H_iH$ and $V_iV$ polarizations.
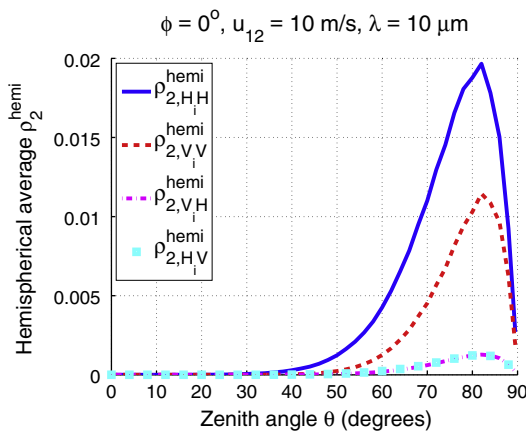
### 4.4. Energy conservation

According to the law of energy conservation, under thermal equilibrium, the energy absorbed by the sea surface equals the energy it radiates. In other words, the sum of the sea surface emissivity and hemispherical reflectivity equals 1, expressed as:

$$\varepsilon + \rho^{hemi} = 1. \tag{33}$$

This criterion is examined for the $H$ and $V$ polarizations, respectively. The results for the up-wind direction $\phi = 0°$ are shown in Fig. 11. Correlation between surface points is not considered. The sea surface emissivity used here is obtained from the model of Li et al. (2012), where 2D surfaces are considered. The reflectivity in $H$ and $V$ polarizations is obtained by:

$$\begin{aligned} \rho_{1,2,H}^{hemi} &= \rho_{1,2,H_iH}^{hemi} + \rho_{1,2,V_iH}^{hemi}, \\ \rho_{1,2,V}^{hemi} &= \rho_{1,2,V_iV}^{hemi} + \rho_{1,2,H_iV}^{hemi}. \end{aligned} \tag{34}$$

When only the direct emissivity $\varepsilon_0$ and the reflectivity with one reflection $\rho_1$ are taken into account (solid lines in Fig. 11), the energy conservation criterion is fulfilled only for small zenith angles (e.g. $\theta < 40°$). For larger $\theta$, a loss of energy is found because of the negligence of multiple reflections (Yoshimori et al., 1994), with a maximum being about 0.059 in $H$ polarization and 0.046 in $V$ polarization around $\theta \approx 80°$, meaning that 5.9% and 4.6% of the incident energy in $H$ and $V$ polarizations are lost, respectively.

The criterion of energy conservation is better fulfilled after taking into account the emissivity with one reflection $\varepsilon_1$ (dashed lines in Fig. 11). The maxima of the losses of energy are reduced to 0.035 in $H$ polarization and 0.024 in $V$ polarization.

The losses of energy decrease even more after taking into account the hemispherical reflectivity with two reflections $\rho_2^{hemi}$ (dashed-dotted lines in Fig. 11). The maxima of the losses of energy are reduced to 0.015 in $H$ polarization and 0.012 in $V$ polarization.

It should be pointed out that the loss of energy obtained here is more significant than that obtained by Li et al. (2013) with 1D surface models. A maximum of loss of energy about 4% in $\varepsilon_0 + \rho_1^{hemi}$ is reported by Li et al. (2013), when multiple surface reflections are ignored. After taking into account $\varepsilon_1$ and $\rho_2^{hemi}$, the energy is nearly conserved for all $\theta$, with the maximum of loss of energy being less than 0.005, which is one third of that obtained by the 2D surface models here. This implies that multiple surface reflections of higher orders must be more significant for 2D surfaces for large zenith angles $\theta$.

## 5. Conclusion and discussion

Surface reflections are important phenomena when deriving the sea surface infrared reflectivity. This paper analytically calculates the infrared reflectivity of sea surfaces with Gaussian slope PDF, by taking into account the first and second reflections by the surface. To evaluate the occurrence of the double reflections, a bistatic illumination function is developed. The cross-polarization effect is also studied.

It is shown that, for a given incidence direction, the bidirectional surface reflectivity with one and two reflections is distributed around the global plane of incidence but shifted toward the horizon with respect to the global specular reflection direction. Cross polarizations in reflectivity with one and two reflections are weak. The hemispherical reflectivity with two reflections is significant for large zenith angles $\theta$. The energy conservation is then examined. A loss of energy is observed by the models when multiple surface reflections are ignored, with maxima being about 0.059 in $H$ polarization and 0.046 in $V$ polarization. The criterion of energy conservation is better fulfilled after taking into account



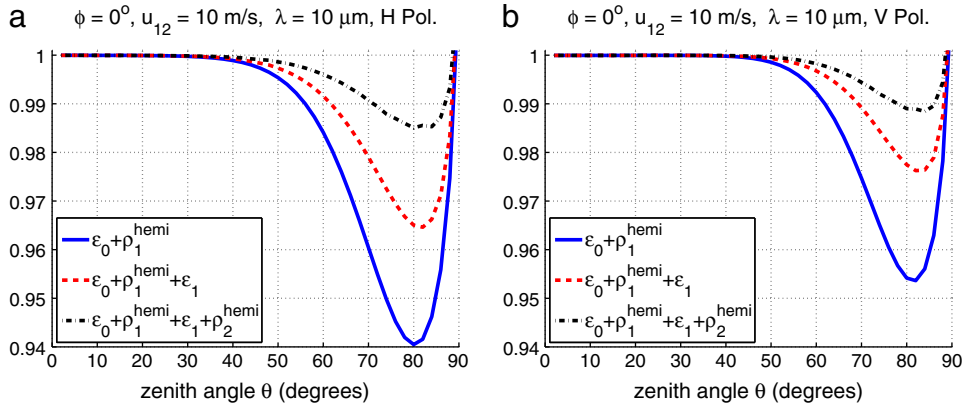**Fig. 10.** Hemispherical reflectivity with two surface reflections is shown versus the zenith angle $\theta$. The sensor is located in the up-wind direction $\phi = 0°$. The wind speed is $u_{12} = 10$ m/s, and the wavelength is $\lambda = 10 \, \mu m$.

**Fig. 11.** Check of energy conservation in *H* (a) and *V* (b) polarizations, for the same parameters as in Fig. 10.

the emissivity with one reflection $\varepsilon_1$ and the hemispherical reflectivity with two reflections $\rho_2^{\text{hemi}}$.

If sensors sensitive to polarization are available, it would be possible to measure the bidirectional reflectivity in four polarizations by emitting a *H* or *V* polarized incident ray. For emitters located near the zenith, it is even possible to evaluate only the contribution of the first reflection, as $\rho_1$ is much larger in these directions (maxima of the order of $10^{-3}$) than $\rho_2$ (maxima of the order of $10^{-7}$).

On the other hand, by comparing Figs. 9, 5 and 6, we can find that the cross-polarized bidirectional reflectivity with one reflection $\rho_1$ and that with two reflections $\rho_2$ have very different features in the global plane of incidence: $\rho_1$ equals zero whereas $\rho_2$ does not. Besides, it can be predicted that the cross-polarized bidirectional reflectivity with more reflections does not equal zero in this plane either. This feature makes it possible to measure the contribution of multiple ($\geq 2$) surface reflections.

As the bidirectional reflectivity is derived, this work can be applied to cases in which the radiance of the background is anisotropic, for example, with multiple emitters.

## Appendix A. Rotation angles $\alpha$ and $\alpha_i$

According to the law of reflection, $\hat{s}_i$, $\hat{s}$ and $\hat{n}_0$ belong to the same plane (called the plane of incidence). As a result, the direction of the local horizontal polarization $h_0$ and that of $h_{0,i}$ are identical, as they are both perpendicular to the plane of incidence. The directions of the $H_i$, $H$ and $h_0$ polarizations are given by:

$$\hat{u}_{H_i} = \hat{s}_i \times \hat{z}, \hat{u}_H = \hat{s} \times \hat{z}, \hat{u}_{h_0} = \hat{s} \times \hat{n}_0, \tag{A.1}$$

respectively, where $\hat{u}$ stands for the unitary vector in the direction of the corresponding polarization state. The rotation angles $\alpha_i$ and $\alpha$ are then given by:

$$cos\alpha_i = \hat{u}_{H_i} \cdot \hat{u}_{h_0}, cos\alpha = \hat{u}_H \cdot \hat{u}_{h_0}, \tag{A.2}$$

respectively.

## Appendix B. Integration over the Dirac delta function

The integration in Eq. (11) involves integrations over two Dirac delta functions. To perform these two integrations, the variables of integration have to be changed from $d\gamma_{x_0} d\gamma_{x_0}$ to $d\theta_i^{-,\text{spe}} d\phi_i^{-,\text{spe}}$. This section details the calculation of these two integrations.

The unitary normal vector $n_0$ of $M_0$ can be expressed as:

$$\hat{n}_0 = \frac{\hat{s}_i^{-,\text{spe}} + \hat{s}}{2 \cos \chi_0}. \tag{B.1}$$

Then, the slopes of $M_0$ can be expressed by the *x*, *y*, and *z* components of $\hat{n}_0$ as follows:

$$\gamma_{x_0} = -\frac{\hat{n}_{1,x}}{\hat{n}_{1,z}} = -\frac{\sin\theta_i^{\text{spe}} \cos\phi_i^{\text{spe}} + \sin\theta \cos\phi}{\cos\theta_i^{\text{spe}} + \cos\theta}, \tag{B.2}$$

$$\gamma_{y_0} = -\frac{\hat{n}_{1,x}}{\hat{n}_{1,z}} = -\frac{\sin\theta_i^{\text{spe}} \sin\phi_i^{\text{spe}} + \sin\theta \sin\phi}{\cos\theta_i^{\text{spe}} + \cos\theta}, \tag{B.3}$$

The change of variables is then performed, and the variables of integration in Eq. (11) become:

$$d\gamma_{x_0} d\gamma_{y_0} = J \, d\theta_i^{\text{spe}} d\phi_i^{\text{spe}}, \tag{B.4}$$

where *J* is the Jacobian of the transformation, given by:

$$\begin{aligned} J &= \left| \frac{d\gamma_{x_0}}{d\theta_i^{\text{spe}}} \frac{d\gamma_{x_0}}{d\phi_i^{\text{spe}}} - \frac{d\gamma_{y_0}}{d\theta_i^{\text{spe}}} \frac{d\gamma_{y_0}}{d\phi_i^{\text{spe}}} \right| \\ &= \frac{\sin\theta_i^{\text{spe}}}{(\cos\theta_i^{\text{spe}} + \cos\theta)^3} \left[ 1 + \cos\theta_i^{\text{spe}} \cos\theta \right. \\ &\quad \left. + \sin\theta_i^{\text{spe}} \sin\theta \cos(\phi_i^{\text{spe}} - \phi) \right] | \end{aligned} \tag{B.5}$$

The integrations over $\theta_i^{\text{spe}}$ and $\phi_i^{\text{spe}}$ result in:

$$\rho_{1,A,B}(\theta, \phi, \theta_i, \phi_i) = \frac{\rho_{1,A,B}^{\text{local}} g_0 J(\theta, \phi, \theta_i, \phi_i)}{\Lambda(\theta) + \Lambda^-(\theta_i) + 1} \tag{B.6}$$

## References

Bourlier, C., Berginc, G., & Saillard, J. (2002). Monostatic and bistatic statistical shadowing functions from a one-dimensional stationary randomly rough surface: II. Multiple scattering. *Waves in Random Media, 12,* 175–200.

Bourlier, C., Saillard, J., & Berginc, G. (2000). Effect of correlation between shadowing and shadowed points on the Wagner and Smith monostatic one-dimensional shadowing functions. *IEEE Transactions on Antennas and Propagation, 48,* 437–446.

Bourlier, C., Saillard, J., & Berginc, G. (2000). Intrinsic infrared randiation of the sea surface. *Progress in Electromagnetics Research, 27,* 185–335.

Bourlier, C., Saillard, J., & Berginc, G. (2001). Theoretical study on two-dimensional Gaussian rough sea surface emission and reflection in the infrared frequencies with shadowing effect. *IEEE Transactions on Geoscience and Remote Sensing, 39,* 379–392.

Caillault, K., Fauqueux, S., Bourlier, C., Simoneau, P., & Labarre, L. (2007). Multiresolution optical characteristics of rough sea surface in the infrared. *Applied Optics*, *46*, 5471–5481.

Cox, C., & Munk, W. (1954). Measurement of the roughness of the sea surface from photographs of the sun's glitter. *Journal of the Optical Society of America*, *44*, 838–850.

Fauqueux, S., Caillault, K., Simoneau, P., & Labarre, L. (2009). Multiresolution infrared optical properties for Gaussian sea surfaces: Theoretical validation in the one-dimensional case. *Applied Optics*, *48*, 5337–5347.

Hale, G. M., & Querry, M. R. (1973). Optical constants of water in the 200-nm to 200-μm wavelength region. *Applied Optics*, *12*, 555–563.

Henderson, B. G., Theiler, J., & Villeneuve, P. (2003). The polarized emissivity of a wind-roughened sea surface: A Monte Carlo model. *Remote Sensing of Environment*, *88*, 453–467.

Leskova, T. A., Maradudin, A. A., & Novikov, I. V. (2000). Scattering of light from the random interface between two dielectric media with low contrast. *Journal of the Optical Society of America A*, *17*, 1288–1300.

Li, H., Pinel, N., & Bourlier, C. (2011). A monostatic illumination function with surface reflections from one-dimensional rough surfaces. *Waves in Random and Complex Media*, *21*, 105–134.

Li, H., Pinel, N., & Bourlier, C. (2012). Polarized infrared emissivity of 2D sea surfaces with one surface reflection. *Remote Sensing of Environment*, *124*, 299–309.

Li, H., Pinel, N., & Bourlier, C. (2013). Polarized infrared reflectivity of one-dimensional Gaussian sea surfaces with surface reflections. *Applied Optics*, *52*, 6100–6111.

Lynch, P. J., & Wagner, R. J. (1970). Rough-surface scattering: Shadowing, multiple scatter, and energy conservation. *Journal of Mathematical Physics*, *11*, 3032–3042.

Masuda, K. (2006). Infrared sea surface emissivity including multiple reflection effect for isotropic Gaussian slope distribution model. *Remote Sensing of Environment*, *103*, 488–496.

Nalli, N. R., Minnett, P. J., & Delst, P. (2008). Emissivity and reflection model for calculating unpolarized isotropic water surface-leaving radiance in the infrared. I: Theoretical development and calculations. *Applied Optics*, *47*, 3701–3721.

Nalli, N. R., Smith, W. L., & Huang, B. (2001). Quasi-specular model for calculating the reflection of atmospheric-emitted infrared radiation from a rough water surface. *Applied Optics*, *40*, 1343–1353.

Ross, V., Dion, D., & Potvin, G. (2005). Detailed analytical approach to the Gaussian surface bidirectional reflectance distribution function specular component applied to the sea surface. *Journal of the Optical Society of America A*, *22*, 2442–2453.

Sancer, M. (1969). Shadow-corrected electromagnetic scattering from a randomly rough surface. *IEEE Transactions on Antennas and Propagation*, *17*, 577–585.

Schott, P., de Beaucoudrey, N., & Bourlier, C. (2003). Reflectivity of one-dimensional rough surfaces using the ray tracing technique with multiple reflections. *Geoscience and Remote Sensing Symposium, 2003. IGARSS'03. Proceedings. 2003 IEEE International, Vol. 7*. (pp. 4214–4216).

Smith, B. (1967). Geometrical shadowing of a random rough surface. *IEEE Transactions on Antennas and Propagation*, *15*, 668–671.

Smith, W. L., Knuteson, R. O., Revercomb, H. E., Feltz, W., Nalli, N. R., Howell, H. B., et al. (1996). Observations of the infrared radiative properties of the ocean implications for the measurement of sea surface temperature via satellite remote sensing. *Bulletin of the American Meteorological Society*, *77*, 41–51.

Su, W., C., T. P., & R., K. (2002). Observations of reflectance distribution around sunglint from a coastal ocean platform. *Applied Optics*, *41*, 7369–7383.

Vaitekunas, D. A., Alexan, K., Lawrence, O. E., & Reid, F. (1996). SHIPIR/NTCS: A naval ship infrared signature countermeasure and threat engagement simulator. *Proceedings of SPIE*, *2744*, 411–424.

Watts, P. D., Allen, M. R., & Nightingale, T. J. (1996). Wind speed effects on sea surface emission and reflection for the along track scanning radiometer. *Journal of Atmospheric and Oceanic Technology*, *13*, 126–141.

Wu, X., & Smith, W. L. (1997). Emissivity of rough sea surface for 8–13 μm: Modeling and verification. *Applied Optics*, *36*, 2609–2619.

Yoshimori, K., Itoh, K., & Ichioka, Y. (1994). Thermal radiative and reflective characteristics of a wind-roughened water surface. *Journal of the Optical Society of America A*, *11*, 1886–1893.